LETTER

doi:10.1038/nature23893

# Tunable interacting composite fermion phases in a half-filled bilayer-graphene Landau level

A. A. Zibrov[1], C. Kometter[1], H. Zhou[1], E. M. Spanton[2], T. Taniguchi[3], K. Watanabe[3], M. P. Zaletel[4] & A. F. Young[1]

**Non-Abelian anyons are a type of quasiparticle with the potential to encode quantum information in topological qubits protected from decoherence[1]. Experimental systems that are predicted to harbour non-Abelian anyons include p-wave superfluids, superconducting systems with strong spin–orbit coupling, and paired states of interacting composite fermions that emerge at even denominators in the fractional quantum Hall (FQH) regime. Although even-denominator FQH states have been observed in several two-dimensional systems[2–4], small energy gaps and limited tunability have stymied definitive experimental probes of their non-Abelian nature. Here we report the observation of robust even-denominator FQH phases at half-integer Landau-level filling in van der Waals heterostructures consisting of dual-gated, hexagonal-boron-nitride-encapsulated bilayer graphene. The measured energy gap is three times larger than observed previously[3,4]. We compare these FQH phases with numerical and theoretical models while simultaneously controlling the carrier density, layer polarization and magnetic field, and find evidence for the paired Pfaffian phase[5] that is predicted to host non-Abelian anyons. Electric-field-controlled level crossings between states with different Landau-level indices reveal a cascade of FQH phase transitions, including a continuous phase transition between the even-denominator FQH state and a compressible composite fermion liquid. Our results establish graphene as a pristine and tunable experimental platform for studying the interplay between topology and quantum criticality, and for detecting non-Abelian qubits.**

At high magnetic fields, two-dimensional electrons form flat bands known as Landau levels. At finite charge density $n$, interactions drive the formation of ordered states that depend on the Landau-level filling ($\nu = 2\pi\ell_B^2 n$, where $\ell_B = \sqrt{\hbar/(eB)}$ is the magnetic length, $e$ is the elementary charge and $\hbar$ is the reduced Planck constant) and the spin and orbital structure of the Landau-level wavefunctions. Of particular interest is the fate of the half-filled Landau level, which can be understood as a weakly interacting state of composite fermions[6] that consist of one electron and two magnetic flux quanta. Having incorporated part of the external magnetic field $B$, the composite fermions experience an effective field $B_{\mathrm{eff}} = B(1 - 2\nu)$. At $\nu = 1/2$, this field vanishes and the composite fermions form an emergent Fermi surface[7] that manifests in both microwave and transport experiments[8,9]. As in a conventional metal, the emergent Fermi surface can be unstable, depending on the strength and sign of the residual interactions between the composite fermions. Most intriguingly, composite fermions have been predicted to form the quantum Hall analogue of a superconductor[5,10], which, in a single-component system, naturally has p-wave pairing symmetry and supports non-Abelian, charge-$e$/4 quasiparticle excitations in an incompressible liquid. Numerical studies find that in the lowest Landau level of a conventional, massive electron system, the composite-fermion interactions are sharp and the Fermi surface is stable, whereas in the first Landau level a node in the single-particle wavefunction leads to softer composite-fermion interactions that are conducive to pairing[11]. An incompressible quantized Hall state was indeed observed[2] in the first Landau level of GaAs quantum wells, at filling $\nu = 5/2$, although experiments have yet to reveal definitive evidence for non-Abelian statistics.

Bernal-stacked bilayer graphene (BLG) is emerging as a new platform for exploring the half-filled Landau level. Comprising two aligned graphene layers in direct contact, it has a rich phase diagram that depends on both the electron density $n$ and the layer polarization density $p$. An FQH phase was observed[3] at $\nu = -1/2$ in BLG devices suspended in vacuum and gated from below. The interpretation of this state[12] is complicated by the complex structure of the zero-energy Landau level (ZLL) of BLG, which consists of eight quasi-degenerate components comprising electron spin, a 'valley' index that is characteristic of honeycomb systems, and an orbital degeneracy that is unique to BLG. The spin and valley combine to form an approximately SU(4) isospin, whereas no such symmetry relates the orbital levels, which are approximately equivalent to the lowest ($N = 0$) and first excited ($N = 1$) Landau levels of conventional, massive electrons. Although a non-Abelian paired state is expected theoretically when the fractional part of the filling lies in a single $N = 1$ orbital, this is difficult to verify experimentally in a singly gated sample. In devices in which the BLG is sandwiched between boron nitride, it can be gated from above and below, and the splitting between valley and orbital degrees of freedom can then be controlled using magnetic and electric fields[13,14]. A recent experiment[15] exploited this control to map out the valley and orbital character of the ZLL, revealing that, throughout much of the accessible parameter space, the valence electrons are fully polarized in a single valley and orbital component. However, even-denominator states have not previously been reported in dual-gated devices.

Here we report magnetocapacitance measurements from a new generation of BLG devices, depicted schematically in Fig. 1a. Unlike previous dual-gated device architectures[13–15], the gate electrodes on both sides of the BLG are made of few-layer graphite flakes, greatly reducing sample disorder (see Supplementary Fig. 11). The sum and difference of the two applied gate voltages, $n_0$ and $p_0$ (see Fig. 1), control the charge density $n$ and layer polarization density $p$ within the bilayer. Figure 1b shows the penetration field capacitance $C_{\mathrm{P}}$, which is closely related to the thermodynamic compressibility[16], in a region of the $n_0$–$p_0$ plane that spans the ZLL, $-4 < \nu < 4$. Incompressible FQH phases manifest as peaks in $C_{\mathrm{P}}$ that are locked to the filling factor. We observe many new incompressible states at fractional $\nu$ and numerous $p_0$-tuned phase transitions at which the state becomes compressible at fixed $\nu$.

We group the observed FQH sequences into three categories on the basis of the pattern of incompressible phases, indicated by red, blue and green colouring in Fig. 1c. In the red regions, we observe sequences of FQH states at valence fillings of $\tilde{\nu} \equiv \nu - \lfloor\nu\rfloor = m/(2m+1)$. In contrast, in the blue regions, we observe robust FQH states only at $\tilde{\nu} = 1/3$, 2/3 and 1/2, with weaker states observed at $\tilde{\nu} = 7/13$ and 3/5 (Fig. 1d, e).

[1]Department of Physics, University of California, Santa Barbara, California 93106, USA. [2]California Nanosystems Institute, University of California at Santa Barbara, Santa Barbara, California 93106, USA. [3]Advanced Materials Laboratory, National Institute for Materials Science, Tsukuba, Ibaraki 305-0044, Japan. [4]Department of Physics, Princeton University, Princeton, New Jersey 08544, USA.

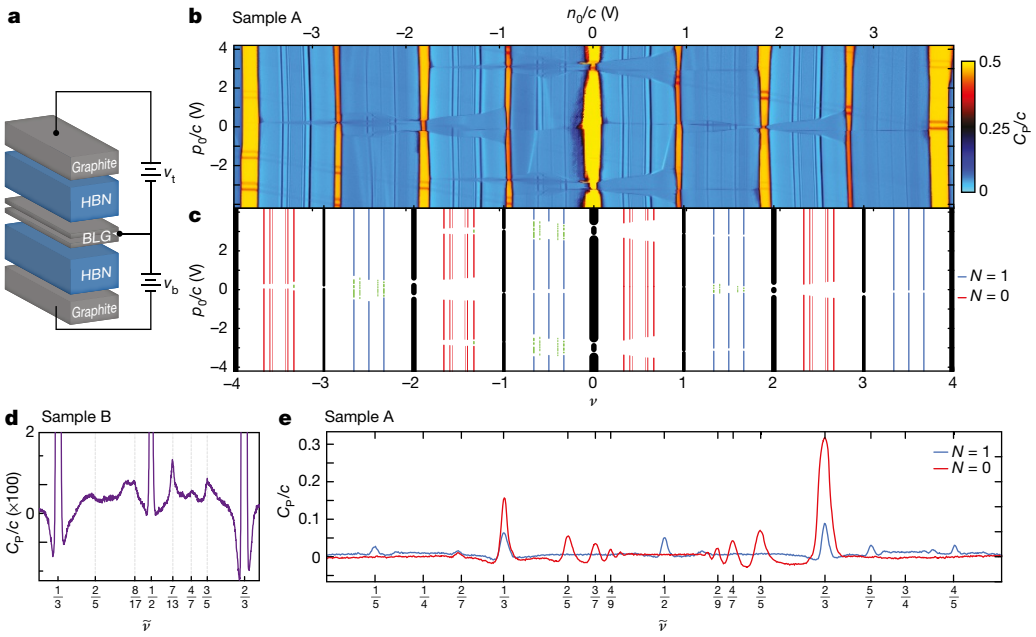


**Figure 1 | Fractional quantum Hall (FQH) effect in an all van der Waals heterostructure. a**, Device schematic. A BLG flake is successively encapsulated in hexagonal boron nitride (HBN) dielectric and graphite gate layers. Charge density $n$ and layer polarization density $p$ are controlled via voltages $n_0/c \equiv (v_t + v_b)$ and $p_0/c \equiv (v_t - v_b)$, where $c$ is the average geometric capacitance of the two gates to the graphene, and $v_t$ and $v_b$ are the applied gate voltages. **b**, Penetration-field capacitance $C_P$ at $B = 12$ T from sample A. The plot spans the ZLL, showing incompressible quantum Hall states, manifesting as peaks in $C_P$, at all integer filling factors $\nu$ as well as at several rational $\nu$. **c**, Illustration of the orbital character of the observed FQH states. As valence electrons fill $N = 0$ orbitals (red), we observe odd-denominator fractions consistent with two-flux composite-fermion hierarchy states. When filling $N = 1$ orbitals (blue), only multiples of 1/3 appear consistently from this sequence, with the second most robust state occurring at half-filling. Near orbital and valley level crossings (green), a cascade of interlayer correlated states is observed[19]. **d**, Detail of an $N = 1$ Landau level from a second device (sample B), measured at $B = 14$ T and base temperature. Incompressibility peaks are evident at $\tilde{\nu} = 3/5$ and 7/13, but not 2/5 or 6/13, showing the development of particle–hole asymmetry. **e**, FQH sequences in valence $N = 0$ and $N = 1$ regions as a function of $\tilde{\nu} \equiv \nu - \lfloor \nu \rfloor$ for $1 < \nu < 2$ (blue) and $2 < \nu < 3$ (red), measured at $p_0/c = -2.0$ V and $p_0/c = -2.7$ V, respectively, in sample A. The $N = 0$ levels are compressible at half-filling, whereas the $N = 1$ levels show incompressibility peaks.

The red and blue regions correspond to the experimentally[15] determined orbital character ($N = 0$ or $N = 1$) of the valence electrons, which have different effective interactions. In red regions, a single $N = 0$ component is fractionally filled and the effective interactions are sharp, stabilizing the odd-denominator sequence that is associated with integer quantum Hall states of two-flux composite fermions. We therefore ascribe the compressible state at $\tilde{\nu} = 1/2$ to the composite Fermi liquid (CFL). In the blue regions, a single $N = 1$ component is fractionally filled and the effective interactions are softer. This suggests that the incompressible state observed at $\tilde{\nu} = 1/2$ is an FQH state constructed from paired composite fermions. Finally, in the green regions, $p_0$ induces a level crossing between the eight near-degenerate components[15], and there is a cascade of phase transitions between incompressible states with a structure that depends on the fractional filling.

We first discuss the even-denominator FQH states. In an incompressible FQH state, a finite energy is required to inject an electron or hole. This 'thermodynamic' gap can be determined[16] from $C_P$, shown in Fig. 2a for different temperatures at $B = 14$ T. We measure this thermodynamic gap by integrating the inverse electronic compressibility $\partial\mu/\partial n$ with respect to $n$ (Fig. 2b), yielding a gap of 4 K at the base temperature of our dilution refrigerator (see Supplementary Information). Transport measurements from a second device show the expected quantized Hall plateau and concomitant longitudinal resistance minimum (Fig. 2c). Temperature-dependent transport exhibits a lower value of the activation gap of $1.8 \pm 0.2$ K at $B = 14$ T. This discrepancy is not surprising[16]. The thermodynamic gap measures the energy that is required to add an entire electron–hole pair, whereas thermally activated transport measures the energy cost of injecting a fractionally charged quasiparticle–quasihole pair. For a half-filled FQH state, the quasiparticle charge is predicted to be $e/4$, in which case the measured activation gap should be roughly one-quarter of the thermodynamic gap[16] at $T = 0$.

In a bilayer electron system it is natural to ask whether the incompressible states observed at half-filling are single- or multi-component phases. Whereas the leading theoretical candidates for a single-component even-denominator FQH phase—the paired Pfaffian[5] and anti-Pfaffian[17,18] states—are non-Abelian, in multi-component systems the Abelian '331' phase is more likely[19]. Using the map of the valence polarization[15] (aspects of which were repeated here at higher resolution; see Supplementary Information), we find that the gapped phase appears in regions where the fractional filling is polarized into a single $N = 1$ component. The situation is thus roughly analogous to the $\nu = 5/2$ state of GaAs (ref. 2), in which numerics have long predicted a paired phase. We note, however, that the measured activation gap is several times larger than the largest gaps measured in GaAs (558 mK; ref. 20), ZnO (90 mK; ref. 4) or suspended BLG (600 mK; ref. 3).

Despite the superficial similarity, the $N = 1$ orbital in BLG differs in two important ways from its counterpart in semiconductor quantum wells. First, the $N = 1$ Landau levels of BLG and GaAs are not strictly equivalent. In GaAs, the $N = 1$ Landau level consists purely of the conventional $|1\rangle$ orbital wavefunction. In contrast, in BLG, the $N = 1$ Landau level includes a combination of both $|0\rangle$ and $|1\rangle$ wavefunctions localized on different sublattices of the unit cell (see Supplementary Information), with the relative weight of the $|0\rangle$ wavefunction growing with $B$. The effective interaction depends on the character of the wavefunction, so that $B$ tunes the structure of electron–electron interactions continuously within an $N = 1$ level. At low $B$ the wavefunctions are purely $|1\rangle$-like, with comparatively soft interactions, whereas at high $B$ they are an equal admixture of $|0\rangle$ and $|1\rangle$ and interactions are consequently sharper. Numerical studies predict that a non-Abelian paired phase at lower $B$ should give way to a gapless CFL at sufficiently high magnetic fields[12,21] (Fig. 2d). We indeed find that the $\tilde{\nu} = 1/2$ gap changes non-monotonically with $B$ (Fig. 2e), peaking around $B = 27$ T

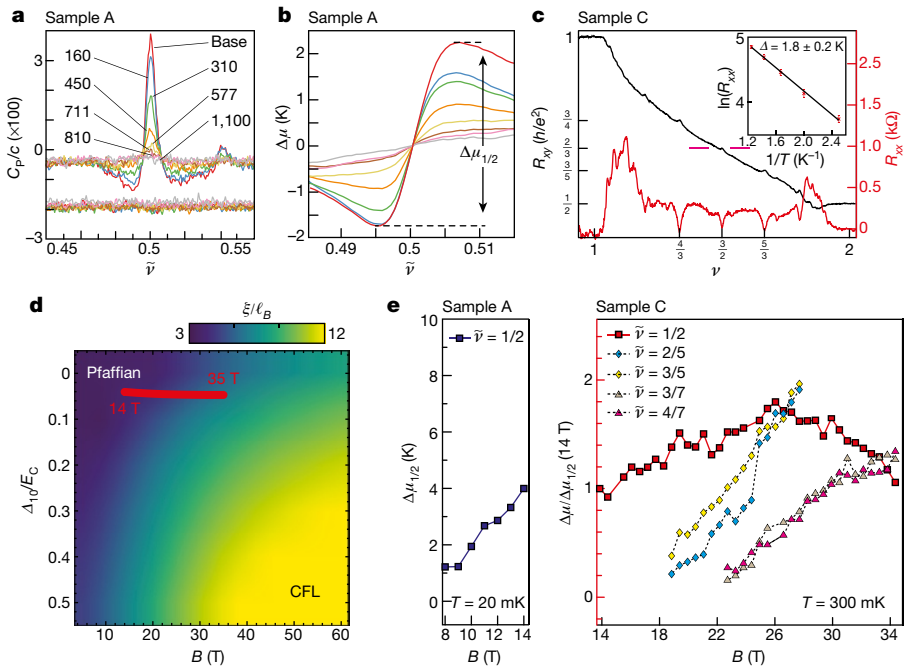


**Figure 2 | The $\tilde{\nu} = 1/2$ state. a**, Penetration-field capacitance $C_P$ (top curves) and dissipation (bottom curves) near $\nu = 3/2$ at $B = 14$ T (sample A). The labels denote the probe temperature in millikelvin. **b**, Density dependence of the chemical potential $\Delta\mu \approx (e/k_B)\int(C_P/c)\mathrm{d}(n_0/c)$, obtained by integrating the curves in **a**. $\Delta\mu_{1/2}$ is defined as the difference between the maximum and minimum $\Delta\mu$ proximal to $\nu = 3/2$. **c**, Hall (black; $R_{xy}$) and longitudinal (red; $R_{xx}$) resistance measured in sample C. Magenta lines denote $R_{xy} = 2/3$. Inset, Arrhenius plot of $R_{xx} \approx e^{-\Delta/(2T)}$ at $\nu = 3/2$, from which we obtain $\Delta = 1.8 \pm 0.2$ K at $B = 14$ T. Error bars in the gap measurement arise primarily from ambiguity in choosing the thermally activated region. **d**, DMRG calculation of the correlation length $\xi$ at $\tilde{\nu} = 1/2$ in the $N = 1$ level as a function of the energy splitting $\Delta_{10}$ between the $N = 0$ and $N = 1$ orbitals, in units of Coulomb energy $E_C$, and the magnetic field $B$ (see Supplementary Information). In the lower right corner, the system transitions from the incompressible Pfaffian phase to the compressible CFL phase. The red line denotes an estimate[15] of the trajectory within the $B$–$\Delta_{10}$ plane corresponding to the data shown in **e**. **e**, The thermodynamic gap $\Delta\mu_{1/2}$ at different $B$ in sample A (left) and sample C (right). Data in the right panel are scaled to the $\Delta\mu_{1/2}$ gap at $B = 14$ T (see Supplementary Information). For energy gaps of other FQH states, see Supplementary Fig. 17 and Supplementary Tables 1 and 2.

and then decaying up to the limit of our experiment at $B = 35$ T. Over a similar range, we simultaneously observe the emergence of a conventional odd-denominator FQH series typical of the lowest Landau level, providing further evidence that the effective $N = 1$ interactions sharpen with magnetic field (see Supplementary Information and Supplementary Fig. 16). The decrease in the $\tilde{\nu} = 1/2$ gap despite an increase in the Coulomb scale $E_C \propto \sqrt{B}$ supports the scenario of a paired-to-CFL transition[22] at higher magnetic fields.

Second, particle–hole symmetry breaking differs in BLG as compared with GaAs. Within a single Landau level, the Pfaffian and anti-Pfaffian states, which can be understood as different pairing channels, are degenerate owing to a particle–hole symmetry (effected by $\tilde{\nu} \leftrightarrow 1 - \tilde{\nu}$). Including scattering between Landau levels breaks this symmetry and determines the ground state. Although the subject of longstanding debate, recently demonstrated numerical agreement between exact diagonalization and density matrix renormalization group (DMRG) methods suggests that the $\nu = 5/2$ state of GaAs is in the anti-Pfaffian phase[23–25]. However, Landau-level scattering is markedly different in BLG: scattering between the ZLL and the $|N| \geq 2$ levels breaks particle–hole symmetry only weakly, whereas scattering within the ZLL breaks it strongly as a result of the small splitting between $N = 0$ and $N = 1$ levels ($\Delta_{10} \approx 0.1E_C$; see Supplementary Information). In our experiment, particle–hole symmetry breaking manifests in the fractions observed in the $N = 1$ Landau level. We find incompressible states at $\tilde{\nu} = 7/13$ and 3/5 (Fig. 1d), the particle–hole conjugates of what is observed in GaAs, in which unconventional states were observed[20] at 6/13 and 2/5. To address these differences, we perform comprehensive DMRG calculations that account for the $B$-dependent mixed orbital character and screening from filled $|N| \geq 2$ Landau levels, while non-perturbatively accounting for scattering between the $N = 0$ and $N = 1$ orbitals of the ZLL (Fig. 2; see Supplementary Information for computational details). We find that, in contrast to GaAs (refs 23–25), the Pfaffian phase is strongly preferred over the anti-Pfaffian phase over the experimentally explored range of $p_0$ and $B$. In agreement with this finding, we observe a strong incompressible phase at 7/13 (as well as a weaker feature at 8/17), the predicted filling of the first 'daughter' state of the Pfaffian phase[26]. In contrast, the anti-Pfaffian daughter states are expected at 6/13 and 9/17, at which no incompressible states are observed.

Our results suggest that encapsulated BLG has certain advantages over GaAs as a platform for interferometric detection of non-Abelian quasiparticles[11]. First, the large energy gap and small correlation length relative to GaAs may reduce bulk–edge coupling that is detrimental to interferometric probes[27], while exponentially suppressing the density of thermally activated quasiparticles. Second, hexagonal boron nitride gate dielectrics can be made almost arbitrarily thin, enabling edges and quantum point contacts to be engineered using sharp electrostatic potentials. Recent experiments have demonstrated long coherence lengths in the quantum Hall regime along such gate-defined edges[28]. Finally, the putative Pfaffian state at $\nu = -1/2$ in BLG would have fewer edge modes than the anti-Pfaffian state at $\nu = 5/2$ in GaAs, making the former a preferable candidate for interferometry. Even without phase-coherent transport measurements, the thermodynamic measurements presented here, carried to lower temperatures, can be used to probe topological ground-state degeneracy[29], which could provide clear evidence for non-Abelian statistics in the near future.

In addition to control over the total charge density $n$ and the effective interactions, the dual-gated architecture allows us to tune level crossings between the eight components of the ZLL. Within the ZLL, the two valleys are supported on opposite layers, so the electric field ($p_0$) acts like a 'valley Zeeman' field and the layer polarization density ($p$) can be used to infer valley polarization. A schematic of the single-particle

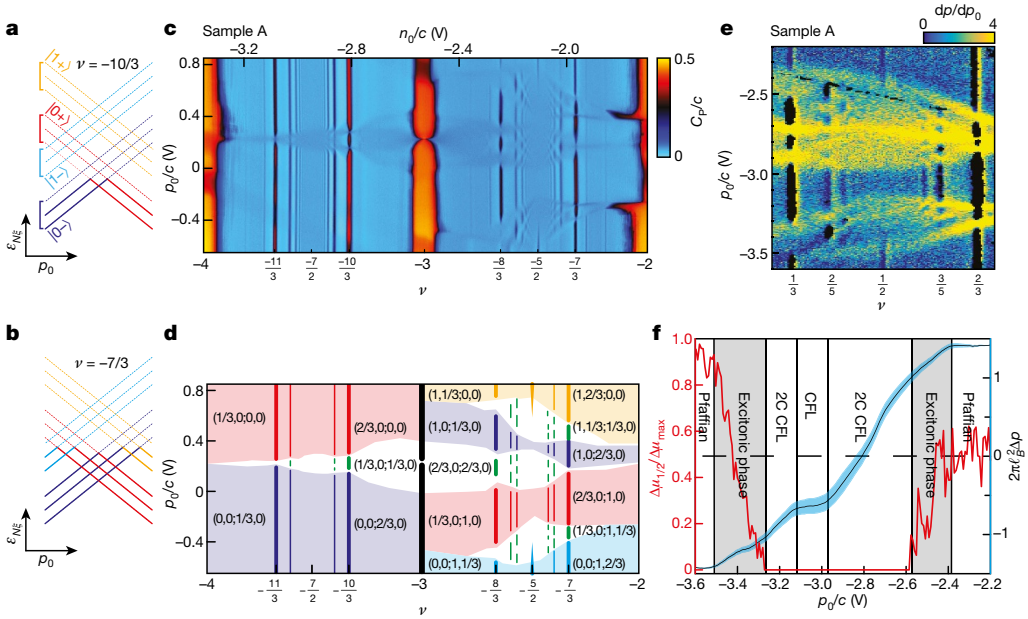


**Figure 3 | Interlayer correlated FQH states. a**, **b**, Single-particle energy level ($\varepsilon_{N\xi}$) crossing and level-filling diagram as a function of $p_0$, for $\nu=-10/3=-4+2/3$ (**a**) and $\nu=-7/3=-4+5/3$ (**b**). Occupation of the levels in increments of $\nu=1/3$ is represented by schematically showing each Landau level (indicated by colour) as being divided into three branches. Three distinct phases are expected by filling the two lowest-lying 'branches' (solid lines) in **a**. In **b**, crossings now involve $N=0$ and $N=1$ levels, and six distinct phases are expected. **c**, Measured $C_P$ for $-4<\nu<-2$ near $p_0/c=0$ at $B=12$ T in sample A. **d**, Annotated phase diagram for the range depicted in **c**. Occupations of the four relevant orbitals ($\nu_{0+}$, $\nu_{1+}$; $\nu_{0-}$, $\nu_{1-}$) are indicated for each fractional multiple of 1/3. Shaded areas correspond to regions where the fractional filling lies entirely within one orbital. Colouring follows the schemes in **a** and **b**. **e**, Layer polarizability $dp/dp_0$, measured over an analogous quadruple level crossing at high negative $p_0$ for $-1<\nu<0$ in sample A. **f**, The black curve shows the integrated change in polarization $2\pi\ell_B^2\Delta p=2\pi\ell_B^2\int\partial p/\partial p_0\,dp_0$, measured in the regions immediately adjacent to $\tilde{\nu}=1/2$, with shading indicating $1\sigma$ confidence interval (see Supplementary Information). The red curve shows the $\tilde{\nu}=1/2$ charge gap $\Delta\mu_{1/2}/\Delta\mu_{\max}$. Vertical lines demarcate distinct regimes distinguished by their compressibility and polarizability: the incompressible and unpolarizable regions are the Pfaffian phase; incompressible but polarizable regions are the excitonic phase discussed in the main text; compressible but polarizable regions are presumably two-component (2C) CFLs; and the compressible and unpolarizable is a one-component CFL.

energies near $p_0\approx0$ is shown in Fig. 3a, b. Four single-particle levels are involved in the crossing, which we label by their orbital ($N=0$, $N=1$) and valley ($\xi=\pm$) indices (we suppress the spin here, because tilt $B$-field measurements show that the spin polarization is unchanged across the transition). Because the two valleys are distinguished by their crystal momentum, the tunnelling between them vanishes in the absence of short-range disorder and the crossing between the levels is unavoided, as supported by the sharp transition at $\nu=-3$ and $p_0\approx0$ (Fig. 3c). Hence, unlike the dependence on $B$, the $p_0$ dependence across the transition is not equivalent to continuously tuning the interaction potential. When charge is separately conserved in each valley, the valley polarization cannot change continuously without closing the neutral gap: just as the charge gap vanishes in a compressible system, the neutral gap vanishes in a polarizable system. During such depolarization, the charge gap may or may not close.

Figure 3c shows $C_P$ near $p_0=0$. For the best-developed odd-denominator $\tilde{\nu}=m/(2m+1)$ states when $-4<\nu<-3$, $|m|+1$ distinct high-$C_P$ incompressible regions are visible, separated by $|m|$ low-$C_P$ transitions. Referring to Fig. 3a, the crossing is predicted to transfer valence filling $m/(2m+1)$ between $N=0$ orbitals in opposite valleys. The $m$ compressibility spikes presumably occur when filling $1/(2m+1)$ is transferred between valleys. This is expected from composite Fermion theory, which predicts two-component correlated states[6,19] at fillings of $(\nu_+,\nu_-)=(m_+,m_-)/[2(m_++m_-)+1]$ (the '$\pm$' subscripts indicate the valley $\xi=\pm$), separated by phase transitions at which the gap closes. For instance, the state at $\nu=-4+2/3$ and $p_0=0$ corresponds to $m_\pm=-1$ and we ascribe it to a previously unobserved valley SU(2) singlet. For $-3<\nu<-2$, states at filling $\nu=-4+(3m+1)/(2m+1)$ exhibit $3m+1$ transitions. Four levels are involved in these transitions. At high $p_0$, one $N=0$ level is completely filled and the fractional filling resides in the $N=1$ level of the same valley. As $p_0$ is decreased, occupation is transferred according to the levels shown in Fig. 3b, consistent with the observed strengths of the gapped phases, the $C_P$ peaks of which are strongest when only $N=0$ orbitals are involved.

For odd-denominator states, the high compressibility that is observed when the system changes polarization indicates that the gap for charged excitations also closes. This is not always the case at $\tilde{\nu}=1/2$, at which the charge gap in the single-component $N=1$ regimes at large and small $p_0$ fades gradually into the level crossing. We can quantify this transition by measuring the layer polarization directly (see Supplementary Information). Figure 3e shows the layer polarizability $\partial p/\partial p_0$ over a similar region of four-level crossings. In contrast to the odd-denominator fractions, for which the spikes in polarizability are concentrated on the spikes in compressibility, near $\tilde{\nu}=1/2$ there is a region of $p_0$ where the polarization changes only gradually while the charge gap remains finite. Figure 3f shows the measured charge gap alongside the integrated change in layer polarization across the level crossing. The charge gap persists from valley valence fillings of $(\nu_+,\nu_-)=(1.5,0)$ to $(1.33,0.17)$.

The coexistence of polarizability and incompressibility has intriguing implications. In the clean limit, in which charge is conserved separately in each valley (a limit supported by the sharp transition at $\nu=-3$ and $p_0\approx0$), finite polarizability requires a vanishing neutral gap, implying the existence of a new phase: a gapless fractionalized insulator. Microscopically, because the layers are atomically close, the finite polarization presumably arises from a finite density of inter-valley (equivalently, inter-layer) excitons, and the finite polarizability implies that these neutral excitons are gapless. This behaviour is reminiscent of quantum Hall bilayers at $\nu=1$, for which a charge gap also coexists with

a vanishing neutral gap. The transition is thus distinct in microscopic character from the Pfaffian-to-CFL transition that is predicted at high $B$ in a single-component level (Fig. 2e), during which the charge and neutral gap would vanish in tandem.

Theoretically, the accompanying fractionalization at $\tilde{\nu} = 1/2$ leaves several possibilities for the ultimate collective ground state—and indeed even the quantum statistics—of inter-valley excitons[30]. Most simply, the incompressible exciton phase could be disorder-dominated: as charge is transferred between valleys, the resulting density of excitons is trapped by local potential variations in a mechanism similar to that which stabilizes FQH plateaus over a finite range of $\nu$. However, as is evident in Fig. 2b, c, the even-denominator state is stable to pure charge doping up to only $\Delta\nu \approx 0.005$, more than an order of magnitude less than the change in occupation ($\Delta\nu_+ \approx 0.17$) of the $N = 1$ orbital that is implied by the depolarization measurement. Without this mechanism, the incompressible exciton phase may host phenomena such as inter-layer phase coherence or an emergent Fermi surface, which can be distinguished experimentally by probing thermal transport or inter-layer Coulomb drag.

**Data Availability** The data that support the findings of this study are available from the corresponding author on reasonable request.

**Received 5 November 2016; accepted 26 July 2017.**


1. Kitaev, A. Yu. Fault-tolerant quantum computation by anyons. *Ann. Phys.* **303,** 2–30 (2003).
2. Willett, R. *et al.* Observation of an even-denominator quantum number in the fractional quantum Hall effect. *Phys. Rev. Lett.* **59,** 1776–1779 (1987).
3. Ki, D.-K., Fal'ko, V. I., Abanin, D. A. & Morpurgo, A. F. Observation of even denominator fractional quantum Hall effect in suspended bilayer graphene. *Nano Lett.* **14,** 2135–2139 (2014).
4. Falson, J. *et al.* Even-denominator fractional quantum Hall physics in ZnO. *Nat. Phys.* **11,** 347–351 (2015).
5. Moore, G. & Read, N. Nonabelions in the fractional quantum Hall effect. *Nucl. Phys. B* **360,** 362–396 (1991).
6. Jain, J. K. Composite-fermion approach for the fractional quantum Hall effect. *Phys. Rev. Lett.* **63,** 199–202 (1989).
7. Halperin, B. I., Lee, P. A. & Read, N. Theory of the half-filled Landau level. *Phys. Rev. B* **47,** 7312–7343 (1993).
8. Willett, R. L., Ruel, R. R., West, K. W. & Pfeiffer, L. N. Experimental demonstration of a Fermi surface at one-half filling of the lowest Landau level. *Phys. Rev. Lett.* **71,** 3846–3849 (1993).
9. Kang, W., Stormer, H. L., Pfeiffer, L. N., Baldwin, K. W. & West, K. W. How real are composite fermions? *Phys. Rev. Lett.* **71,** 3850–3853 (1993).
10. Read, N. & Green, D. Paired states of fermions in two dimensions with breaking of parity and time-reversal symmetries and the fractional quantum Hall effect. *Phys. Rev. B* **61,** 10267–10297 (2000).
11. Nayak, C., Simon, S. H., Stern, A., Freedman, M. & Das Sarma, S. Non-Abelian anyons and topological quantum computation. *Rev. Mod. Phys.* **80,** 1083–1159 (2008).
12. Papić, Z. & Abanin, D. A. Topological phases in the zeroth Landau level of bilayer graphene. *Phys. Rev. Lett.* **112,** 046602 (2014).
13. Lee, K. *et al.* Chemical potential and quantum Hall ferromagnetism in bilayer graphene. *Science* **345,** 58–61 (2014).
14. Maher, P. *et al.* Tunable fractional quantum Hall phases in bilayer graphene. *Science* **345,** 61–64 (2014).
15. Hunt, B. M. *et al.* Direct measurement of discrete valley and orbital quantum numbers in bilayer graphene. *Nat. Commun.* (in the press).
16. Eisenstein, J. P., Pfeiffer, L. N. & West, K. W. Compressibility of the two-dimensional electron gas: measurements of the zero-field exchange energy and fractional quantum Hall gap. *Phys. Rev. B* **50,** 1760–1778 (1994).
17. Levin, M., Halperin, B. I. & Rosenow, B. Particle-hole symmetry and the Pfaffian state. *Phys. Rev. Lett.* **99,** 236806 (2007).
18. Lee, S.-S., Ryu, S., Nayak, C. & Fisher, M. P. A. Particle-hole symmetry and the $\nu = 5/2$ quantum Hall state. *Phys. Rev. Lett.* **99,** 236807 (2007).
19. Halperin, B. I. Theory of the quantized Hall conductance. *Helv. Phys. Acta* **56,** 75–102 (1983).
20. Kumar, A., Csáthy, G. A., Manfra, M. J., Pfeiffer, L. N. & West, K. W. Nonconventional odd-denominator fractional quantum Hall states in the second Landau level. *Phys. Rev. Lett.* **105,** 246808 (2010).
21. Apalkov, V. M. & Chakraborty, T. Stable Pfaffian state in bilayer graphene. *Phys. Rev. Lett.* **107,** 186803 (2011).
22. Metlitski, M. A., Mross, D. F., Sachdev, S. & Senthil, T. Cooper pairing in non-Fermi liquids. *Phys. Rev. B* **91,** 115111 (2015).
23. Rezayi, H. R. & Simon, S. H. Breaking of particle-hole symmetry by Landau level mixing in the $\nu = 5/2$ quantized Hall State. *Phys. Rev. Lett.* **106,** 116801 (2011).
24. Zaletel, M. P., Mong, R. S. K., Pollmann, F. & Rezayi, E. H. Infinite density matrix renormalization group for multicomponent quantum Hall systems. *Phys. Rev. B* **91,** 045115 (2015).
25. Rezayi, E. H. Landau level mixing and the ground state of the $\nu = 5/2$ quantum Hall effect. *Phys. Rev. Lett.* **119,** 026801 (2017).
26. Levin, M. & Halperin, B. I. Collective states of non-Abelian quasiparticles in a magnetic field. *Phys. Rev. B* **79,** 205301 (2009).
27. von Keyserlingk, C. W., Simon, S. H. & Rosenow, B. Enhanced bulk-edge Coulomb coupling in fractional Fabry–Perot interferometers. *Phys. Rev. Lett.* **115,** 126807 (2015).
28. Wei, D. S. Mach–Zehnder interferometry using spin- and valley-polarized quantum Hall edge states in graphene. *Sci. Adv.* **3,** e1700600 (2017).
29. Cooper, N. R. & Stern, A. Observable bulk signatures of non-Abelian quantum Hall states. *Phys. Rev. Lett.* **102,** 176807 (2009).
30. Barkeshli, M., Nayak, C., Papic, Z., Young, A. & Zaletel, M. Fractionalized exciton Fermi surfaces and condensates in two-component quantized Hall states. Preprint at https://arxiv.org/abs/1611.01171 (2016).


**Supplementary Information** is available in the online version of the paper.

**Acknowledgements** We acknowledge experimental assistance of B. Odegard and J. Island, and discussions with M. Barkeshli, C. Dean, E.-A. Kim, R. Mong, C. Nayak, Z. Papic, S. Simon and A. Stern. Magnetocapacitance measurements were funded by the NSF under DMR-1636607. A portion of the nanofabrication and the transport measurements were funded by the ARO under proposal 69188PHH. A.F.Y. acknowledges the support of the David and Lucile Packard Foundation. Measurements above 14 T were performed at the National High Magnetic Field Laboratory, which is supported by National Science Foundation cooperative agreement number DMR-1157490 and the State of Florida. The numerical simulations were performed on computational resources supported by the Princeton Institute for Computational Science and Engineering (PICSciE). E.M.S. acknowledges the support of the Elings Fellowship. K.W. and T.T. acknowledge support from the Elemental Strategy Initiative conducted by the MEXT, Japan and JSPS KAKENHI grant number JP15K21722.

**Author Contributions** A.A.Z., E.M.S. and H.Z. fabricated devices A, B and C, respectively. T.T. and K.W. synthesized the hexagonal boron nitride crystals. A.F.Y. and C.K. built the measurement electronics. A.A.Z., H.Z., E.M.S. and A.F.Y. acquired and analysed the experimental data. M.P.Z. performed the DMRG calculations. A.A.Z., M.P.Z. and A.F.Y. wrote the paper.

**Author Information** Reprints and permissions information is available at www.nature.com/reprints. The authors declare no competing financial interests. Readers are welcome to comment on the online version of the paper. Publisher's note: Springer Nature remains neutral with regard to jurisdictional claims in published maps and institutional affiliations. Correspondence and requests for materials should be addressed to A.F.Y. (andrea@physics.ucsb.edu).

**Reviewer Information** *Nature* thanks D. Abanin, K. Park, K. Yang and the other anonymous reviewer(s) for their contribution to the peer review of this work.